**RAA 2016** Vol. **16** No. **2**, 29 (8pp) doi: 10.1088/1674–4527/16/2/029
*http://www.raa-journal.org* *http://iopscience.iop.org/raa*

***R**esearch in*
***A**stronomy and*
***A**strophysics*

# An improved astrometric calibration technique for space debris observation

Rong-Yu Sun[1,2], Chang-Yin Zhao[1,2] and Yao Lu[1,2,3]

[1] Purple Mountain Observatory, Chinese Academy of Sciences, Nanjing 210008, China; *rysun@pmo.ac.cn*
[2] Key Laboratory of Space Object and Debris Observation, Chinese Academy of Sciences, Nanjing 210008, China
[3] University of Chinese Academy of Sciences, Beijing 100049, China

Received 2015 June 8; accepted 2015 September 10

**Abstract** An optical survey is the main technique for detecting space debris. Due to the specific characteristics of observation, the pointing errors and tracking errors of the telescope as well as image degradation may be significant, which make it difficult for astrometric calibration. Here we present an improved method that corrects the pointing and tracking errors, and measures the image position precisely. The pipeline is tested on a number of CCD images obtained from a 1-m telescope administered by Xinjiang Astronomical Observatory while observing a GPS satellite. The results show that the position measurement error of the background stars is around 0.1 pixel, while the time cost for a single frame is about 7.5 s; hence the reliability and accuracy of our method are demonstrated. In addition, our method shows a versatile and feasible way to perform space debris observation utilizing non-dedicated telescopes, which means more sensors could be involved and the ability to perform surveys could be improved.

**Key words:** techniques: image processing — space vehicles — astrometry — methods: data analysis

## 1 INTRODUCTION

Space debris is defined as artificial non-functional objects orbiting around the Earth (Schildknecht 2007). It has been recognized as a serious danger for operational spacecraft and manned spaceflight, and the growing population is becoming an increasing threat for future space operations, as well as posing some unique challenges in orbital environments (Schildknecht et al. 2004; Musci et al. 2004). Detecting and observing space debris, which refer to surveying space debris and obtaining their precise positions utilizing ground-based or space-based equipment, including optical, radar and laser ranging sensors, can mitigate the risk of collision and improve safety in space missions (Flohrer et al. 2008).

A ground-based optical survey is one of the most effective methods for observing space debris (Hebert et al. 2001). The data reduction technique is similar to the one adopted in ground-based CCD astrometry with wide field imagers, and can also be implemented for observing near Earth objects, e.g. comets, asteroids and minor planets, as well as other transient sources in astronomy (Yanagisawa et al. 2005). In detail, first information about all the sources is extracted from a raw CCD image (Sun & Zhao 2013), with a high precision image centering algorithm (Stone 1989), then the background stars are cross-matched with the ones in a catalog, and the appropriate plate model constants are obtained with them; finally the equatorial coordinates of the objects are derived with these constants.

However, for space debris, which is one kind of fast-moving near Earth object, information about position is the main focus of research, rather than photometric data, although recently a few dedicated works investigating photometry of debris have been carried out (Schildknecht et al. 2008). The observations and data reduction for space debris have some special characteristics, and the process of optimized reduction includes two challenges. First, due to the relative movement between objects and background stars, the images may be elongated as streaks regardless of the observing strategy adopted. In this case, the exposure time of a single CCD frame is limited to prevent the images from showing large trails, which leads to high noise levels and relatively low Signal to Noise Ratio (SNR of the sources (Sun et al. 2013). Moreover, the influence of atmospheric turbulence becomes increasingly evident (Popowicz et al. 2013; Jia et al. 2014). Hence, the extraction of precise information about the source is challenging (Kouprianov 2008), and a reduction technique should be improved to adequately overcome these issues. Second, considering that the angular velocity of space debris with respect to the observer is generally high, especially for objects in low Earth orbit, during exposure the telescope should move with the same velocity to track the object; hence effects of the pointing errors and tracking errors may be significant, which makes it difficult to perform stellar cross-match and affects the precision of the plate model (Sun et al. 2015). In addition, because the field of view for a telescope used to observe space debris is generally

wide, the geometric distortion of the CCD plane cannot be ignored. Furthermore, due to the high frame rate in observations, space debris surveys produce large CCD image databases; generally the sizes are beyond the scope of manual investigation, therefore, the data reduction should be performed automatically, with no manual operations or other a priori information provided, and the time consumption should also be optimized to handle data in real-time and discover new objects in an efficient manner. All these factors should be considered to improve the technique adopted during the data reduction process.

In our paper, an improved astrometric calibration technique is presented to approach the challenges described above and advance the data reduction process for space debris. In our pipeline, mathematical morphology transformation is adopted in image processing and, with an innovative stellar matching algorithm, the pointing and tracking errors are corrected and the background stars are matched precisely; finally the position measurements of the images are performed with a neighborhood-centering algorithm. Our method is tested on the CCD images obtained from a 1-m telescope administered by Xinjiang Astronomical Observatory, rather than ones dedicated for observing space debris, and the efficiency and feasibility of our technique are demonstrated in the application. The basic theories of the image processing algorithm as well as the whole pipeline are introduced in Section 2, and their applications on the 1-m telescope are presented in Section 3. The results and discussions are shown in Section 4, and Section 5 gives the conclusion.

## 2 IMAGE PROCESSING ALGORITHM

To solve the problems listed above and optimize the astrometric calibration process for space debris, we made several improvements in the pipeline. For example, a mathematical morphology transformation is made to reduce the image degradation, the positions of background stars are iteratively matched and the precise positions of stars are obtained using a neighborhood-centering algorithm around the theoretical position. The package is implemented in the language C++, based upon a set of C/Fortran libraries. The main reduction process includes the following four steps: mathematical morphology transformation, preliminary source extraction, stellar cross-match and precise source extraction, which are introduced in detail as follows.

### 2.1 Mathematical Morphology Transformation

In several recent studies it has been demonstrated that the mathematical morphology transformation is especially effective in reducing image degradation in observations of space debris, e.g. eliminating the smear noises caused by the absence of a mechanical shutter (Sun et al. 2012a), separating the blended images of the object and background stars (Sun et al. 2012b), and convolving images to improve the quality and astrometric accuracy (Sun et al. 2014). At the beginning of our pipeline, the top-hat operator is adopted, which can be considered as a 2-dimensional convolution in a spatial domain, and a non-linear high-pass filter as well (Laas-Bourez et al. 2012). The top-hat transformation of a grey level image $f(x)$ by structuring element SE is defined as

$$TH^{\mathrm{SE}}(f(x)) = f(x) - O^{\mathrm{SE}}(f(x))\,, \tag{1}$$

where the opening operator $(O(f(x)))$ of a grey level image $f(x)$ by SE is defined as follows, which includes the dilation operator $(D(f(x)))$ and the erosion operator $(E(f(x)))$

$$O^{\mathrm{SE}}(f(x)) = D^{\mathrm{SE}}(E^{\mathrm{SE}}(f(x)))\,, \tag{2}$$

$$\begin{cases} D^{\mathrm{SE}}(f(x)) = \max\{f(x+y) : y \in \mathrm{SE}\} \\ E^{\mathrm{SE}}(f(x)) = \min\{f(x+y) : y \in \mathrm{SE}\}. \end{cases} \tag{3}$$

The dilation operator assigns the maximum value of pixel-values in the structural element to the investigated pixel, while the erosion operator assigns the minimum one. The opening operator first performs the erosion transformation on the image, then applies the dilation transformation. Based on the opening operator, the top-hat transformation first applies the opening operation and then subtracts the operated image from the original one.

The top-hat operator enhances or suppresses information with various applications in the image, according to the geometric structure elements given as the empirical prior information. After transformation, signals having different geometry with the structural elements can be preserved, and other information in the image is eliminated. With an appropriate structure element, the top-hat transformation reduces the background variations of the raw CCD images, and leads to a smoother image, which is more feasible to apply a global threshold and image segmentation. In our pipeline, the mathematical morphology transformation is adopted to prepare the image for the preliminary source extraction. We should notice that the scope of our work is not only the image processing technique itself, but also the application in combination with other advanced techniques on data reduction, hence the detailed characteristics of the mathematical morphology transformation are beyond our discussion.

### 2.2 Preliminary Source Extraction

After image convolution, the sources in images are extracted preliminarily, which means the sources extracted here are not used for precise astrometry, but for correcting the pointing errors and tracking errors as well as the distortions in the cross-match process. It should be noted that we may obtain precise source information directly using other techniques, e.g. SExtractor (Bertin & Arnouts 1996) or DAOPHOT (Stetson 1987), however, these methods are inefficient and less effective from some point of view. First, due to the specific characteristics of images, lots of spurious detections may be obtained if no dedicated optimizations are made, which make it difficult for the following

data reduction process, and if additional algorithms are introduced to clean these detections, extra run time is needed. Second, for space debris observations, not all sources in the image are needed to derive the precise plate model; in most cases the number of background stars may reach several thousand due to the large field of view, however only part of them are used, e.g. the ones brighter than 12 mag, the number of which is generally around several hundred.

Considering that in this step we do not need highly precise position measurements, just approximate ones are sufficient, a global threshold and segmentation are performed with a relatively high threshold level, which is defined as several times the level of fluctuations above the background level. Then a two path union-finding algorithm is adopted to detect the connected pixel groups, and the ones with more than a specific number of pixels are identified as individual objects. Finally, the pixel groups of the bright objects in the image are obtained, and the ones that represent discrete noise are discarded; a simple barycenter method is adopted to estimate the image positions $(x_o, y_o)$ in pixel coordinates.

### 2.3 Stellar Cross-match

As described above, this step is the key to the whole pipeline. It is important to match the background stars precisely when geometric distortions and telescope pointing errors may be present. Considering that photometric information about the images is not accurate due to image degradation, only positional information is utilized in the cross-match process. At first we search all the stars in the catalog around the pointing coordinates of the telescope (of course they are approximate), with a three times larger field of view, and a transformation is made to obtain the star position $(\xi, \zeta)$ on the tangent plane from the equatorial plane $(\alpha, \delta)$,

$$\begin{cases} \xi = \dfrac{\cos\delta \sin(\alpha-\alpha_0)}{\sin\delta \sin\delta_0+\cos\delta \cos\delta_0 \cos(\alpha-\alpha_0)} \\ \zeta = \dfrac{\sin\delta \cos\delta_0-\cos\delta \sin\delta_0 \cos(\alpha-\alpha_0)}{\sin\delta \sin\delta_0+\cos\delta \cos\delta_0 \cos(\alpha-\alpha_0)} \end{cases} , \quad (4)$$

where $(\alpha_0, \delta_0)$ is the equatorial position of the telescope pointing. It should be noted that this typical gnomonic projection is valid for most telescopes, but for Schmidt telescopes, the projection equation is different. Truncating the high-order items, the projection can be expressed as

$$\begin{cases} \xi\prime = \xi - \frac{1}{3}\xi\prime(\xi\prime^2 + \zeta\prime^2) \\ \zeta\prime = \zeta - \frac{1}{3}\zeta\prime(\xi\prime^2 + \zeta\prime^2) \end{cases} , \quad (5)$$

where $(\xi\prime, \zeta\prime)$ are the results for Schmidt telescopes. $(\xi, \zeta)$ are obtained from Equation (4) directly, and $(\xi\prime, \zeta\prime)$ can be calculated iteratively.

Then with the pixel scale, the pixel positions $(x_c, y_c)$ of background stars are obtained, and all the stars are sorted according to their distances to the center of the image. Taking the set of star positions from the catalog as $C$, and the set of extracted positions as $O$, the cross-match process is performed iteratively.

(1) We pick the first two stars of $C$, which are the nearest to the center of the image, and obtain the pixel range between them as $d_1$, then all the sources extracted in $O$ are checked to find pairs of sources with distances close to $d_1$. These pairs are taken as candidates. If no pairs are found, the next star in $C$ will be picked to repeat the process until the candidate pairs are found.

(2) The next star in $C$ is selected and the distances between the first two stars and it are obtained as $d_{11}$ and $d_{12}$, then all the sources in $O$ are checked again to find the one with approximate distances $d_{11}$ and $d_{12}$, which means the three sources form the same triangle as the ones from the catalog. If there is more than one triangle, the next star from $C$ will be adopted to find four extracted sources configuring a quadrilateral. An initial set of transformation coefficients is derived

$$\begin{aligned} x_o &= a_1 + a_2 x_c + a_3 y_c \,, \\ y_o &= b_1 + b_2 x_c + b_3 y_c \,, \end{aligned} \quad (6)$$

where $(a_1, a_2, a_3, b_1, b_2, b_3)$ are the coefficients which reduce the linear deviations caused by the pointing and tracking errors. It should be noticed that although the plate constants can be obtained with the few stars matched above, the number of stars is not adequate for obtaining a precise least squares solution, and the distribution of locations for these stars in the field of view is nonuniform, hence the accuracy of the plate model is affected. In addition, due to the high-order deviations mainly caused by the geometric distortion, the deviation between the theoretical position and the measured one for stars at the edge of the image is significant, which leads to mismatching. We correct the theoretical positions of the stars with the coefficients above, which reduces the linear deviations

$$\begin{aligned} x_{c1} &= a_1 + a_2 x_c + a_3 y_c \,, \\ y_{c1} &= b_1 + b_2 x_c + b_3 y_c \,, \end{aligned} \quad (7)$$

where $(x_{c1}, y_{c1})$ is the initially corrected position.

(3) For all the stars in $C$, an improved neighborhood matching is performed. First a rectangular domain with a fixed size of $B_1 \times B_1$ pixels is set as the range gate by taking $(x_{c1}, y_{c1})$ as the center; if only one extracted star with position $(x_o, y_o)$ is located in the range gate, the two positions are matched. Considering the stars at the edge of an image, the deviations between $(x_{c1}, y_{c1})$ and $(x_o, y_o)$ are more distinct than those for the ones in the middle of an image, hence the value of $B_1$ is generally set large. Then another set of coefficients is derived

$$\begin{aligned} x_o = {} & a_1 + a_2 x_{c1} + a_3 y_{c1} + a_4 x_{c1}^2 + a_5 x_{c1} y_{c1} \\ & + a_6 y_{c1}^2 + a_7 x_{c1}^3 + a_8 x_{c1}^2 y_{c1} + a_9 x_{c1} y_{c1}^2 \\ & + a_{10} y_{c1}^3 \,, \\ y_o = {} & b_1 + b_2 x_{c1} + b_3 y_{c1} + b_4 x_{c1}^2 + b_5 x_{c1} y_{c1} \\ & + b_6 y_{c1}^2 + b_7 x_{c1}^3 + b_8 x_{c1}^2 y_{c1} + b_9 x_{c1} y_{c1}^2 \\ & + b_{10} y_{c1}^3 \,, \end{aligned} \quad (8)$$

where $(a_1, a_2, \ldots, a_{10})$ and $(b_1, b_2, \ldots, b_{10})$ are the coefficients which correct the non-linear deviations.

Then the theoretical positions of the stars are corrected again with them

$$\begin{aligned} x_{c2} = \; & a_1 + a_2 x_{c1} + a_3 y_{c1} + a_4 x_{c1}^2 + a_5 x_{c1} y_{c1} \\ & + a_6 y_{c1}^2 + a_7 x_{c1}^3 + a_8 x_{c1}^2 y_{c1} + a_9 x_{c1} y_{c1}^2 \\ & + a_{10} y_{c1}^3 \,, \\ y_{c2} = \; & b_1 + b_2 x_{c1} + b_3 y_{c1} + b_4 x_{c1}^2 + b_5 x_{c1} y_{c1} \\ & + b_6 y_{c1}^2 + b_7 x_{c1}^3 + b_8 x_{c1}^2 y_{c1} + b_9 x_{c1} y_{c1}^2 \\ & + b_{10} y_{c1}^3 \,, \end{aligned} \tag{9}$$

where $(x_{c2}, y_{c2})$ is the finally corrected theoretical position for background stars. It is notable that $(x_{c2}, y_{c2})$ is much more accurate than $(x_c, y_c)$ due to the corrections of pointing errors, tracking errors and geometric distortion.

### 2.4 Precise Source Extraction

With the corrected theoretical positions of background stars as a priori information, a highly efficient detection method is adopted to obtain the precise measurements of star images. In particular, for each star, a range gate with size $B_2 \times B_2$ pixels is set by taking $(x_{c2}, y_{c2})$ to be the center, and within the given range gate the mean value $m$ and standard deviation $\sigma$ of all the pixels are calculated, then a threshold value is set as $T = m + k \times \sigma$, where $k$ is the value given empirically. Within the range gate, the pixels with values greater than the threshold $T$ are considered to be the signals, and the connected group of these pixels is searched. If the group consists of more than $N_{min}$ pixels, which is set at another threshold, it is taken as the star image, and the following calculations are performed

$$\begin{aligned} I_{\rm gray} &= \sum_{(i,j)\in O} I_{i,j} - T \,, \\ ox &= \sum_{(i,j)\in O} (I_{i,j} - T) \times (i - x_{c2}) \,, \\ oy &= \sum_{(i,j)\in O} (I_{i,j} - T) \times (j - y_{c2}) \,. \end{aligned} \tag{10}$$

Here $O$ is the group of image pixels, while $I_{i,j}$ is the analog to digital unit value of the pixel $(i, j)$, and $ox$ and $oy$ are the first order moments of the star image with respect to $(x_{c2}, y_{c2})$. Then the deviation $(dx, dy)$ of the star image center with respect to the gate center is obtained

$$\begin{aligned} dx &= \frac{ox}{I_{\rm gray}} \,, \\ dy &= \frac{oy}{I_{\rm gray}} \,. \end{aligned} \tag{11}$$

Finally, the precise position $(X, Y)$ of the star image center in the whole image is calculated by a simple translation relation.

$$\begin{aligned} X &= x_{c2} + dx \,, \\ Y &= y_{c2} + dy \,. \end{aligned} \tag{12}$$

## 3 APPLICATION

To test the feasibility and efficiency of our method, we observe a GPS satellite with COSPAR ID 2005-038A, which is moving around the Earth at an altitude of about 20 000 km. A 1-m telescope administered by Xinjiang Astronomical Observatory is utilized in this study. It should be mentioned that because this telescope is not dedicated for space debris observation, the application will show the universality of our technique, and from an economic point of view, a more versatile way to perform debris surveys, which means more telescopes can be involved in debris observations. The 1-m telescope is set on an alt-azimuth mounting, and information about the case being studied is shown in Table 1.

**Table 1** Information about the 1-m Telescope

| | |
|---|---|
| Longitude | 87.17° E |
| Latitude | 43.30° N |
| Altitude | 2037.3 m |
| Field of view | 1.3° × 1.3° |
| Row & Column binning | 2 |
| Readout channels | 4 |
| Size of frame | 2112 × 2068 pixels |
| Spatial sampling | 2.26″ |
| Exposure time | 1000 ms |
| Observation period | 2015/03/25 22:18-22:46 UTC |
| Filter | $B$ & $R$ |

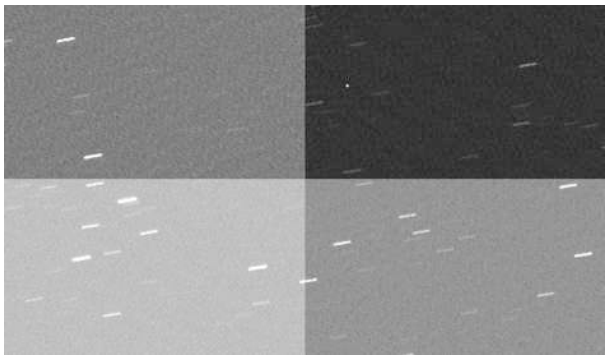

**Fig. 1** A part of the sample raw CCD image acquired in observation.

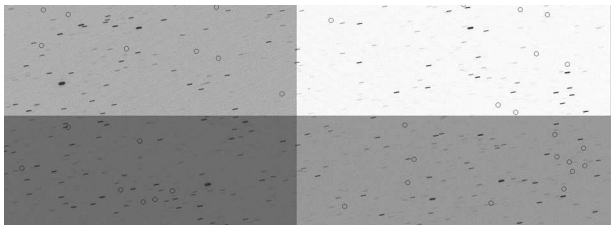

**Fig. 2** The diagram of the pointing errors in the image.

During the process of acquiring images the telescope is tracking the satellite, hence the object appears as a point at the middle of the frame, but the background stars appear as elongated trails. A part of the sample raw CCD image is shown in Figure 1.

Due to the angular velocity associated with the motion of satellites, the exposure time for a single frame is limited, otherwise the images of background stars would be elongated too much, which makes the data reduction more difficult. The whole frame is read out through four channels, leading to variations in the background levels.

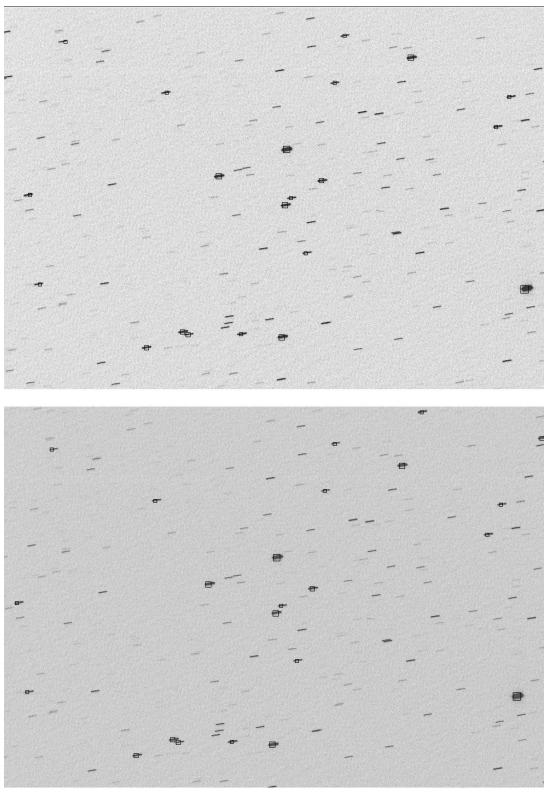

**Fig. 3** The matching result around the location of the initial pair. *Top*: Initial matching. *Bottom*: Iterative matching.

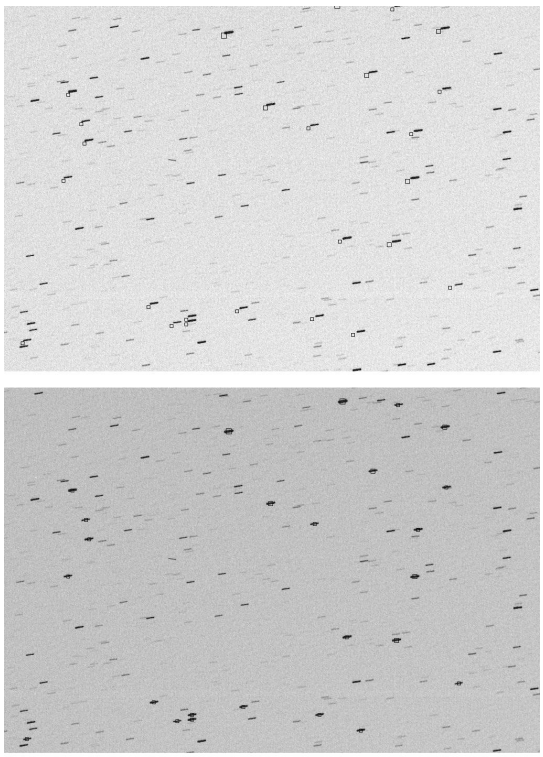

**Fig. 4** The matching result far from the location of the initial pair. *Top*: Initial matching. *Bottom*: Iterative matching.

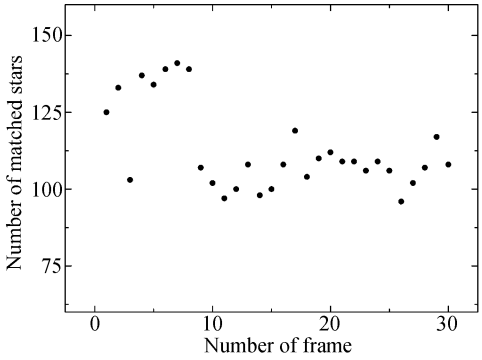


**Fig. 5** The number of the matched background stars for each frame.

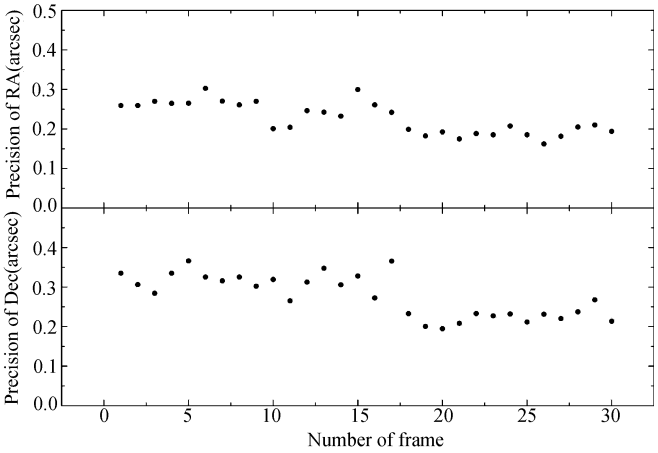


**Fig. 6** The precision of position values for background stars.

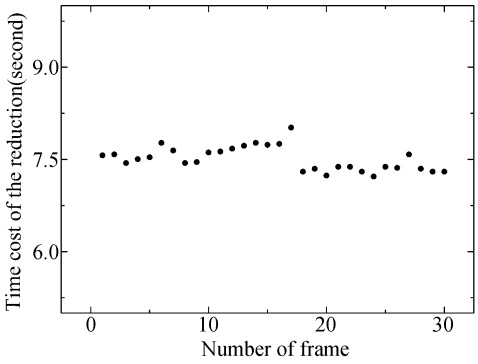


**Fig. 7** The time cost for each frame.

Overall, 31 CCD raw images are acquired, and with these images the astronomical calibration is performed; the measurement accuracy of background stars as well as the time cost is analyzed. In reduction, when applying the mathematical morphology transformation, a structural element with a size of $7 \times 1$ pixels along the line direction is adopted. The small size of the structural element makes the pipeline work faster, and in the preliminary extraction step, the threshold is set as five times the fluctuation level above the background level, while in the precise extraction step, the value is set as $1.5$. The value of $B_1$ is set as $20$ in the cross-match step, and $B_2$ is set as $12$. Stars brighter than

magnitude 12 in the Tycho-2 (Høg et al. 2000) Catalogue are used, and their equatorial coordinates $(\alpha_o, \delta_o)$ obtained by the 20 constant model are compared with the reference ones $(\alpha_c, \delta_c)$, which are obtained directly from the catalog. The resultant deviations $(\sigma_\alpha, \sigma_\delta)$ are calculated as

$$\begin{cases} \sigma_\alpha &= (\alpha_o - \alpha_c) \times \cos\delta_c \,, \\ \sigma_\delta &= \delta_o - \delta_c \,. \end{cases} \tag{13}$$

We take the Root Mean Square (RMS) values of all the deviations in the same image as the precision of reduction. The tests are made on an ordinary business laptop equipped with an Intel Core i7 cpu at 2.3 GHz and 4G of memory, and no parallel optimizations are applied.

## 4 RESULTS AND DISCUSSION

As mentioned above, the pointing and tracking errors while observing space debris utilizing the non-dedicated telescopes are distinct, as shown in Figure 2. The circles mark the theoretical positions of background stars. With a diameter of $10$ pixels, it is easy to find that matching these stars is complicated. The traditional neighborhood matching technique does not work well in this circumstance, and the errors of data reduction may be increased.

The results of the cross-match are shown in Figure 3 and Figure 4. The boxes in the image outline the corrected theoretical positions of the background stars; the top part is the initial matched result and the bottom part is the finally matched one. Figure 3 shows the region where the initial pair of stars is found. It demonstrates that for this region, the high-order deviations are not distinct; however, for other regions far away from it, the influences of the high-order deviations are significant (as shown in Fig. 4), and our innovative iteratively-matching technique works well. All the background stars are matched precisely, which improves the accuracy of the astronomical calibration process.

The number of background stars matched in the reduction process for each CCD frame is shown in Figure 5. As the telescope is tracking the object during exposure, different areas of the sky are targeted, hence the background stars are different as well. It should be noted that these stars are adequate for obtaining the plate constants.

The precision of position values for these stars is shown in Figure 6. The precision of right ascension is around $0.22''$, while that of declination is around $0.27''$. Considering the pixel scale is $2.26''$, the measurement precision of our pipeline is around $0.1$ pixel. These results demonstrate that the pointing and tracking errors are removed, and the background stars are matched correctly, moreover the centroid calculation of the star images is performed precisely.

The time cost of the reduction process for each frame is shown in Figure 7. It can be found that for our $2\mathrm{k} \times 2\mathrm{k}$ frame, the time cost is around 7.5 s; the detailed values are slightly different due to varying matching times in the cross-match process. The results show that it only costs a few seconds to obtain appropriate plate constants from the raw CCD image, which is efficient for data reduction.

Independent of the scientific aspects of the proposed method, another interesting point to consider is the possible economic impact of applying our techniques to optical space debris observation utilizing non-dedicated telescopes. With the improved universal data reduction pipeline, more sensors could be involved in a debris survey, and it could improve the general knowledge related to the population of space debris. Such improvement would also help to better avoid the risk of collision and close encounters between debris and active satellites. However, we should note that it is impossible to test our algorithm under all circumstances, and the deficiencies and limitations should be recognized.

## 5 CONCLUSIONS

In this paper an improved data reduction method is presented for optical space debris observations. In our pipeline the pointing errors and tracking errors of the telescope are considered, and the image degradation is also taken into account for precise position measurement. In particular, a mathematical morphology transformation is adopted for initial processing, and an innovative cross-match algorithm is developed to precisely match the background stars, and finally a neighborhood centering technique is performed to obtain precise values of the plate constants. Our methods are applied to a number of raw CCD images acquired by a 1-m telescope administered by Xinjiang Astronomical Observatory while observing a GPS satellite, and the position measurement errors of background stars are analyzed. The results indicate that when adopting our method, the position measurement precision of the background stars is around 0.1 pixel, which means the plate constants are accurate for astrometry of space debris. Moreover, the processing time for a single $2\mathrm{k} \times 2\mathrm{k}$ frame is about 7.5 s, which makes it capable of real-time data reduction. Furthermore, from an economic point of view, our method represents a versatile and efficient way to perform an optical space debris survey by utilizing non-dedicated telescopes, which means more sensors can be involved and the ability of the whole surveillance network can be improved.

**Acknowledgements** This work was funded by the National Natural Science Foundation of China (Grant Nos. 11125315, 11403108 and 11273069), and the Youth Innovation Promotion Association of CAS (2015252).

## References

Bertin, E., & Arnouts, S. 1996, A&AS, 117, 393

Flohrer, T., Schildknecht, T., & Musci, R. 2008, Advances in Space Research, 41, 1010

Hebert, T. J., Africano, J. L., Stansbery, E. G., et al. 2001, Advances in Space Research, 28, 1283

Høg, E., Fabricius, C., Makarov, V. V., et al. 2000, A&A, 355, L27

Jia, P., Cai, D., & Wang, D. 2014, Experimental Astronomy, 38, 41
Kouprianov, V. 2008, Advances in Space Research, 41, 1029
Laas-Bourez, M., Wailliez, S., Deleflie, F., et al. 2012, Advances in Space Research, 49, 603
Musci, R., Schildknecht, T., & Ploner, M. 2004, Advances in Space Research, 34, 912
Popowicz, A., Kurek, A. R., & Filus, Z. 2013, PASP, 125, 1119
Schildknecht, T. 2007, A&A Rev., 14, 41
Schildknecht, T., Musci, R., & Flohrer, T. 2008, Advances in Space Research, 41, 1039
Schildknecht, T., Musci, R., Ploner, M., et al. 2004, Advances in Space Research, 34, 901
Stetson, P. B. 1987, PASP, 99, 191
Stone, R. C. 1989, AJ, 97, 1227
Sun, R. Y., Lu, Y., & Zhao, C. Y. 2015, Acta Astronomica Sinica, 56, 253
Sun, R.-Y., & Zhao, C.-Y. 2013, RAA (Research in Astronomy and Astrophysics), 13, 604
Sun, R.-y., Zhao, C.-y., Ping, Y.-d., Xiong, J.-n., & Zhang, C. 2012a, Chinese Astronomy and Astrophysics, 36, 340
Sun, R., Zhao, C., & Zhang, Y. 2012b, Science China Physics, Mechanics, and Astronomy, 55, 1945
Sun, R.-Y., Zhao, C.-Y., & Zhang, Y.-P. 2013, PASJ, 65, 110
Sun, R., Zhao, C., & Zhang, X. 2014, AJ, 147, 58
Yanagisawa, T., Nakajima, A., Kadota, K.-I., et al. 2005, PASJ, 57, 399